NEDO-23749
February 1978
Class I

ANALYTICAL MODEL FOR COMPUTING TRANSIENT PRESSURES AND FORCES IN THE SAFETY/RELIEF VALVE DISCHARGE LINE

MARK I CONTAINMENT PROGRAM
TASK NUMBER 7.1.2

A. J. Wheeler

Reviewed: _____
J. M. Healzer, Manager
Containment Methods Unit

Approved: _____
E. Kiss, Manager
Applied Mechanics Section

NUCLEAR ENERGY PROJECTS DIVISION • GENERAL ELECTRIC COMPANY
SAN JOSE, CALIFORNIA 95125

GENERAL ELECTRIC

DISCLAIMER OF RESPONSIBILITY

This document was prepared by or for the General Electric Company. Neither the General Electric Company nor any of the contributors to this document:

A. *Makes any warranty or representation, express or implied, with respect to the accuracy, completeness, or usefulness of the information contained in this document, or that the use of any information disclosed in this document may not infringe privately owned rights; or*

B. *Assumes any responsibility for liability or damage of any kind which may result from the use of any information disclosed in this document.*

TABLE OF CONTENTS

LIST OF ILLUSTRATIONS

LIST OF TABLES

ABSTRACT

An analytical model is described that computes the transient pressures, velocities and forces in the safety/relief valve discharge line immediately after safety/relief valve opening. Equations of motion are defined for the gas-flow and water-flow models. Results are not only verified by comparing them with an earlier version of the model, but also with Quad Cities and Monticello plant data. The model shows reasonable agreement with the earlier model and the plant data.

1. INTRODUCTION

This report describes an analytical model that computes the transient pressures, velocities and forces in the safety/relief valve discharge line (S/RVDL) immediately after safety/relief valve (S/RV) opening.

The technical description of the modeling of the gas flow and water flow systems is presented in Section 2. Section 3 contains verification data, including comparisons with a previous model, and with Quad Cities and Monticello plant data. Section 4 lists references used and Appendices A, B and C provide a definition of symbols used, equations for basic gas dynamics and mass balance across normal shock, respectively.

The model simulates the transient flow of the gas and water in the safety/relief valve discharge line for the period of 0.2 to 0.5 seconds immediately after S/RV opening. Initially the S/RVDL contains air and a water slug at the suppression pool end. When the S/RV opens, steam enters the line, compresses the gas, and expels the water before reaching a steady flow after approximately one second.

The system is represented with two coupled models — one for the gas system and one for the water slug, coupled by virtue of the common pressure and velocity at the gas-water interface. The gas system is treated as a perfect gas for both air and steam. The air-steam interface is followed and different values of k, the ratio of specific heats, are used for the two gas subsystems.

The gas-flow equations are cast in a finite difference form and solved by the method of characteristics, with provision for axial variation of the flow area. The water is modeled with a single, variable volume node. For the water, the one-dimensional momentum equation was integrated axially and solved as a system of ordinary differential equations for flowrate and displacement.

The model also includes several submodels; the more important ones being the submodels for wall condensation and for computation of axial force on the various pipe segments.

2. TECHNICAL DESCRIPTION

2.1 GAS FLOW MODELING

2.1.1 Equations of Motion

The equations of motion for the gases are conservation of mass, momentum and energy. Assuming one-dimensional, unsteady flow and neglecting gravitational effects, the equations are determined to be,

Conservation of Mass:

$$\rho \frac{\partial u}{\partial z} + u \frac{\partial \rho}{\partial z} + \frac{\partial \rho}{\partial t} + \frac{\rho u}{A} \frac{dA}{dz} + \dot{m}''_c \frac{P_w}{A} = 0 \qquad (1)$$

Conservation of Momentum:

$$\rho u \frac{\partial u}{\partial z} + \rho \frac{\partial u}{\partial t} + g_c \frac{\partial P}{\partial z} + g_c \tau_w \frac{P_w}{A} = 0 \qquad (2)$$

Conservation of Energy:

$$\rho \frac{\partial h_o}{\partial t} + \rho u \frac{\partial h_o}{\partial z} - \frac{\partial P}{\partial t} + \dot{Q}'' \frac{P_w}{A} = 0 \qquad (3)$$

These equations distinguish between simple convective heat transfer to the wall and condensation. The dominant mode of heat transfer is condensation and $\dot{Q}''$, the convective heat transfer is assumed to be zero, in the actual model. The convective heat transfer term, $\dot{Q}''$, was included in the documentation of the equation, however.

The model allows for gradual axial variations in the pipe flow area. Sudden expansions or contractions in actual systems must be approximated by more

gradual transitions. The model was tested for area increases up to twice the initial (next to S/RV) pipe area. The area can change at a rate of 20% per node (an S/RV pipe is normally modeled with 100-150 nodes). Within these limits, the mass unbalances during the charging transient were found to be no worse than those with constant area pipes.

A brief outline of the derivations is contained in Appendix A.

2.1.2 Characteristic Equations

The method of characteristics is simple and reliable, and works well with the boundary conditions. When transformed into the characteristic coordinates, the partial differential equations become ordinary differential equations. After inclusion of the perfect gas assumption, the equations become,

$$dP + \frac{\rho C}{g_c}\, du = \alpha\, dt \qquad \text{on } \frac{dt}{dz} = \frac{1}{u + C} \tag{4}$$

$$dP - \frac{\rho C}{g_c}\, du = \beta\, dt \qquad \text{on } \frac{dt}{dz} = \frac{1}{u - C} \tag{5}$$

$$d\rho - \frac{g_c}{C^2}\, dP = \gamma\, dt \qquad \text{on } \frac{dt}{dz} = \frac{1}{u} \tag{6}$$

where

$$\alpha = \frac{C^2}{g_c}\left(-\frac{\rho u}{A}\frac{dA}{dz} - \dot{m}''_c \frac{P_w}{A}\right) + \frac{\rho C}{g_c}\left(-g_c \frac{\tau_w}{\rho A}\right)$$

$$+ \frac{u\tau_w P_w - \dot{Q}'' P_w}{\rho A\left(1/(k-1)\right)} \tag{7}$$

$$\beta = \frac{C^2}{g_c}\left(-\frac{\rho u}{A}\frac{dA}{dz} - \dot{m}''_c\frac{P_w}{A}\right) - \frac{\rho C}{g_c}\left(-g_c\frac{\tau_w}{\rho A}\right)$$

$$+ \frac{u\tau_w P_w - \dot{Q}'' P_w}{\rho A\left(1/(k-1)\right)} \qquad (8)$$

$$\gamma = \frac{-g_c}{C^2}\left(\frac{u\tau_w P - \dot{Q}'' P_w}{\rho A\left(1/(k-1)\right)}\right) \qquad (9)$$

The method of characteristics operates as follows (see the time-space plane in Figure 2-1). With a solution known at time t, for all values of z, a solution is desired at $t + \Delta t$. Characteristics are constructed through the point $(z_n, t + \Delta t)$ using the slopes at points R and L. The line through point R, known as the right traveling characteristic, represents information traveling to the right. Similarly, the line through L represents the left traveling characteristic. Since the locations of R and L are not known until after the characteristics are drawn, interpolation formulae must be manipulated. To obtain the location of points R and L, the characteristic slope is assumed to vary linearly in the appropriate interval (e.g., $z_{n-1} - z_n$ for R). R is then adjusted so that the characteristic passes through point $(z_n, t + \Delta t)$. Having determined the locations of R and L, the corresponding values of u, C, and P are interpolated at points R and L. Equations (4) and (5) are then solved simultaneously for P and u at $(z_n, t + \Delta t)$. Finally, a similar process is used for the 1/u (the path line) characteristics to solve for $\rho(z_n, t + \Delta t)$.

Figure 2-1 also demonstrates the basis for selection of a time step once a value of Δz is chosen. If points R or L fall outside the interval z_{n-1} to z_{n+1}, the numerical method becomes unstable because properties at (z_n, t) have no effect on properties at $(z_n, t + \Delta t)$ when R and/or L are outside the $z_{n-1} - z_{n+1}$ range. The method is most accurate when the locations of R or L coincide with one of the end points of the interval because the least number of time steps minimizes various truncation errors.[1] The model automatically selects a time step on this basis.

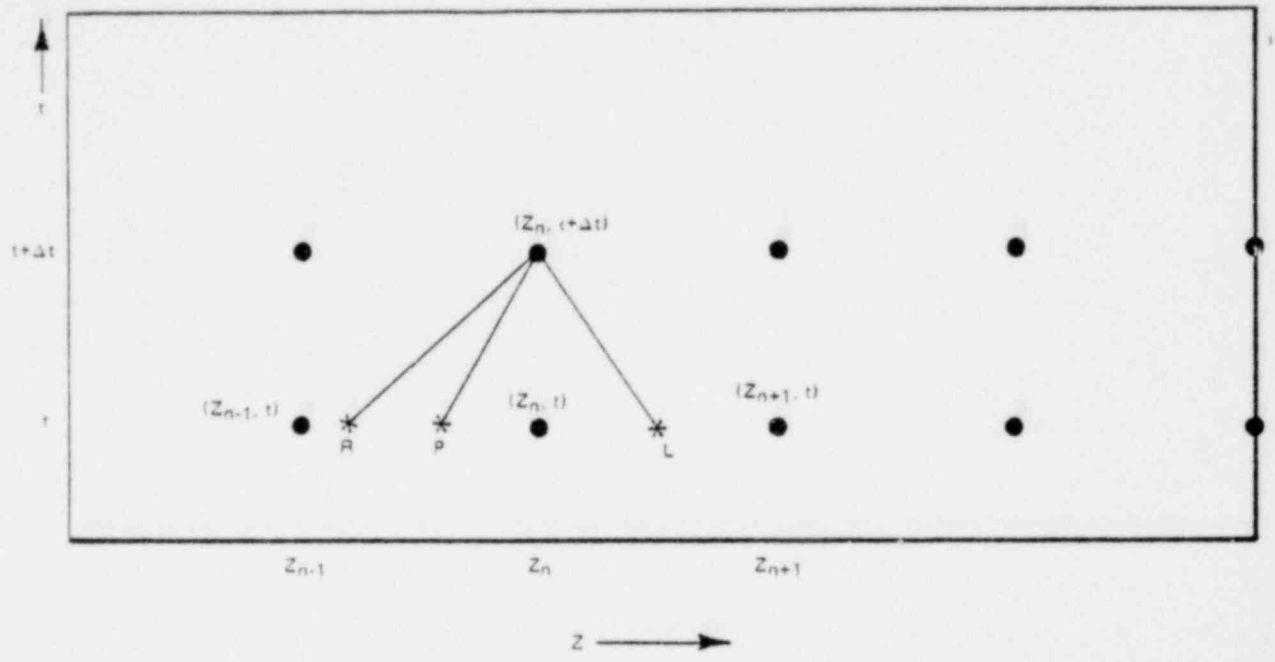

CHARACTERISTICS FOR SUBSONIC FLOW

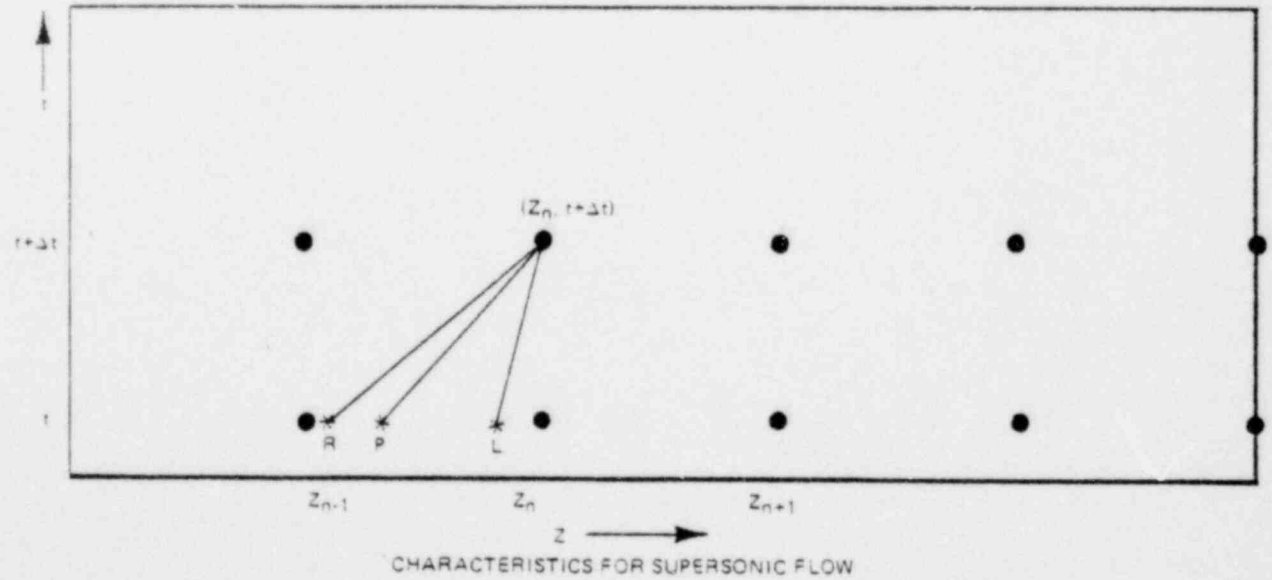

CHARACTERISTICS FOR SUPERSONIC FLOW

Figure 2-1. Construction of Characteristic Lines

2.1.3 Inlet Boundary Conditions

During the entire transient, the flow is assumed to be choked in the S/RV throat and, consequently, the flowrate into the S/RVDL is independent of conditions in the S/RVDL. Furthermore, it is assumed that there are no energy losses as the flow passes through the S/RV. If E denotes S/RVDL entrance conditions and o denotes steamline conditions (low velocity), then

$$h_E + \frac{V_E^2}{2g_c} = h_o, \tag{10}$$

$$h_o = c_p T_o = c_p \frac{P_o}{R\rho_o} = \frac{k}{k-1}\frac{P_o}{\rho_o} \tag{11}$$

$$h_E = \frac{k}{k-1}\frac{P_E}{\rho_E}, \tag{12}$$

and

$$\dot{m} = A_E \rho_E V_E \tag{13}$$

Equations (10), (11), (12), and (13) can be combined to give

$$P_E = \frac{\dot{m}}{A_E}\left(\frac{P_o}{\rho_o}\frac{1}{V_E} - \frac{k-1}{k}\frac{V_E}{2g_c}\right) \tag{14}$$

which is an equation relating P_E and V_E. This equation can be solved simultaneously with the left traveling characteristics equation for P_E and V_E.

2.1.4 Exit Boundary Conditions

During water clearing, gas pressure at the downstream interface from the previous time step is used to drive the water clearing model which, in turn, computes a water velocity. Setting the gas velocity equal to the water velocity, the equation for the right traveling characteristics is then used to compute the new gas pressure.

As the water moves out of the S/RVDL, volume available for the gas increases. When the water has moved a distance equal to the length of a gas node, a new node is added. The mass of gas in the new node is set equal to the gas that flowed out of the adjacent upstream node and the pressure is set equal to that of the adjacent upstream node.

After the water clears, the gas is assumed to accelerate initially to a sonic condition at the exit. If there are other throats upstream of the discharge (i.e., minimums of flow area followed by an expansion), after the decompression wave has moved to the S/RV and back again, the discharge velocity may become supersonic. This occurrence depends on the actual geometry and the possibility is tested for by testing the Mach number at the next to last node. If the next to the last node is supersonic, the sonic exit requirement is relaxed and the last node is permitted to become supersonic.

In some S/RVDL designs the discharge device has a sudden area contraction at the exit (e.g., the perforations in a quencher arm). With the moderate number of nodes used in the model (100-150), this contraction cannot be accurately represented. Instead, an area contraction ratio is specified and isentropic, steady flow[6] is used to connect the last node to the contracted area. When this is done, the flow at the contracted area will become sonic after water clearing and the flow at the last node will be subsonic.

In some designs the exit area is distributed axially (e.g., the perforations down the arms of a quencher). The model treats only one-dimensional flow and the actual system must be approximated as shown in Figure 2-2. This

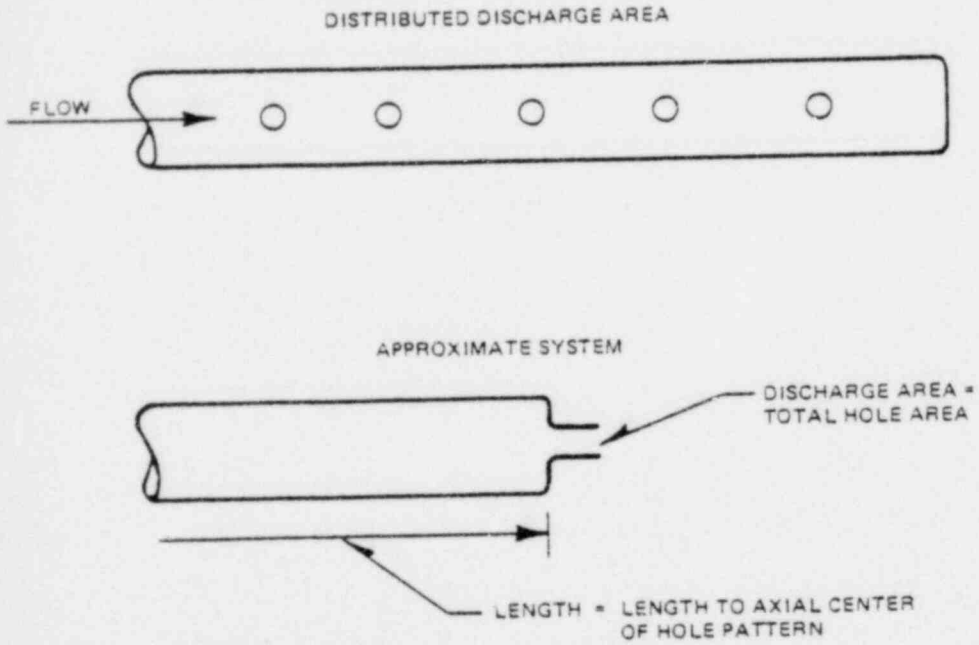

Figure 2-2. Approximation of Distributed Discharge

approximation is considered adequate to compute peak pipe pressures, wave forces and water clearing thrust.

2.1.5 Condensation Model

As the entering steam pushes the original air down the S/RVDL, it comes in contact with the inside pipe wall and partially condenses. Condensation rate is governed by the steam pressure, the wall condensation heat transfer coefficient and the thermal characteristics of the pipe wall.

In computing the amount of condensation, the pipe wall is divided into axial segments, each with a separate heat sink. The radial conduction problem in the pipe wall is solved with the one-dimensional conduction equation,

$$\frac{\partial T}{\partial t} = \alpha' \left(\frac{\partial^2 T}{\partial r^2} + \frac{1}{r} \frac{\partial T}{\partial r} \right) \quad , \tag{15}$$

with a convective boundary at the inside pipe wall and an insulated boundary at the outside pipe wall. The conduction equation is solved with a standard Crank-Nicolson technique.

At the inside pipe wall, the heat transfer is computed from

$$\dot{Q}''_c = h_{wall} (T_{sat} - T_w), \tag{16}$$

where h_{wall} is an input. T_w is the inside pipe wall temperature and T_{sat} is the saturation temperature corresponding to the average steam pressure of the nodes in the segment. This saturation temperature, not the actual temperature, which may be superheated before the flow reaches steady flow, is the appropriate driving temperature.[2] The condensation rate is computed from

$$\dot{m}''_c = \dot{Q}''_c / (h_g - h_L) \quad , \tag{17}$$

where h_g is the enthalpy of the steam at its actual state (possibly superheated condition) and h_L is the liquid enthalpy at the wall temperature.

A computational problem arises when the inside wall of a segment is only partially covered by steam. The original approach was not to initiate any condensation until the segment was half filled with steam. However, this method produced a sudden condensation spike with a resultant artificial pressure disturbance in the S/RVDL. As an alternative, condensation is considered to occur on the entire segment heat slab as soon as the steam reaches the upstream end. However, the effective driving temperature $(T_{sat} - T_w)$, is reduced in direct proportion to the area of pipe wall actually covered relative to the total segment wall area. The resulting total condensation rate is then distributed among those nodes actually containing steam. This method produces a smooth increase in condensation and still maintains the correct energy balance in the steam and pipe wall.

2.1.6 Axial Force Calculations

The forces acting on a piping system can be divided into components (segment forces) to provide a single axial force acting along each segment (Figure 2-3). F.J. Moody[3] has shown that the net segment force on a segment bounded by elbows is

$$F_{seg} = \frac{1}{g_c} \frac{\partial}{\partial t} \int_0^{L_s} \rho A u \, dz \qquad (18)$$

This force can be computed for any bounded segment filled with water or gas by integrating and differentiating the computed velocities and densities. When gas and water are present in the same node, the position of the gas-water interface should be carefully defined to avoid sudden spikes in force.

When a segment discharges to the surroundings, the segment experiences an additional jet thrust, which takes the form

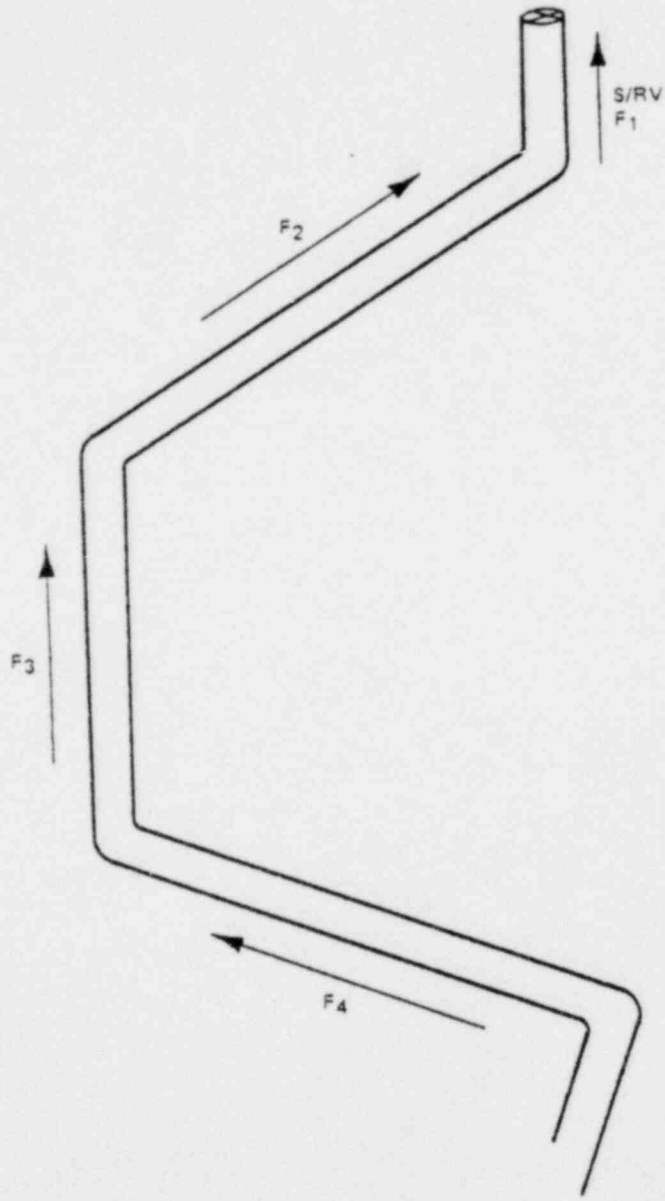

Figure 2-3. Segment Forces

$$F_J = (P_2 - P_\infty) A_2 + \frac{\dot{m}_2 u_2}{g_c} \qquad (19)$$

where location 2 is the open, downstream end of the segment. The total thrust is then the sum of the forces computed by equations (18) and (19).

2.1.7 Supersonic Flow

When the flow becomes supersonic, the sign of the slope of the left traveling characteristic, 1/(u-C), becomes positive, identical to the right traveling characteristic. Consequently, point L falls on the same side of (z_n,t) as point R, as shown in Figure 2-1. This means that point $(z_n, t + \Delta t)$ is unaffected by information at point (z_{n+1},t). In reality, however, moving shock waves can travel upstream into supersonic flow. In the model, if the flow is supersonic at (z_n,t) and subsonic at (z_{n+1},t). In reality, however, moving shock point (z_{n+1},t) and stop. In situations with constant area pipes, supersonic flow rarely occurs, and if it did occur, the Mach number would be close to unity and simplified methods can be used to eliminate the supersonic regions. For pipes with large axial changes in flow area, a more sophisticated approach is required.

A workable solution was arrived at by applying the perfect gas equation for normal shock velocity[6]

$$\frac{P_y}{P_x} = \frac{2k}{k+1} M_x^2 - \frac{k-1}{k+1} \qquad (19)$$

where the subscript x denotes the low pressure or supersonic side and y the high pressure or subsonic side. If n denotes the supersonic node and n+1 the first subsonic node, P_y/P_x is approximated by

$$\frac{P_y}{P_x} = \frac{P_{n+2}}{P_n} \qquad (20)$$

P_{n+2} is used instead of P_{n+1} because the numerical shock is tapered over a two nodes, and use of P_{n+1} would severely underestimate the shock strength.

The resulting shock Mach number is:

$$M_x = \left\{ \frac{k+1}{2k} \left[\frac{P_y}{P_x} + \frac{k-1}{k+1} \right] \right\}^{1/2} \tag{21}$$

and the shock velocity relative to that of the upstream gas is:

$$V_{sr} = M_x C_n \tag{22}$$

The shock velocity relative to the pipe is then:

$$V_s = V_{sr} - u_n \tag{23}$$

In the analytical model, the shock is held stationary for a delay time of

$$t_{delay} = \Delta z / V_s \tag{24}$$

and is then forced upstream by setting:

$$u_n = u_{n+1} \tag{25}$$

$$P_n = P_{n+1} \tag{26}$$

$$\rho_n = \rho_{n+1} \tag{27}$$

During shock delay time, computed mass flows across the shock were found to be unbalanced. To correct this, the independent variables at node n+1 are adjusted.

$$\rho_{n+1} = \rho_{n+2} \tag{28}$$

$$P_{n+1} = P_{n+2} \tag{29}$$

The velocity at n+1 is set to give the correct mass flow (see Appendix B).

$$u_{n+1} = \left(\rho_n u_n A_n - V_s(\rho_{n+2} - \rho_n)A_n\right)/(\rho_{n+1}A_{n+1}) \tag{30}$$

With these changes, the model analyzes supersonic flow with reasonable precision. Specifically, overall mass balances during the changing transient were found to be as good with supersonic flow as when the flow was entirely subsonic.

2.2 WATER FLOW MODELING

2.2.1 Equation of Motion

Water flow is governed by the equation of motion:

$$\frac{\partial w}{\partial t} = \left\{ g_c(P_{Gas} - P_{Pool}) - 0.5\frac{w^2}{\rho_w}\left(\frac{1}{A^2_{pool}} - \frac{1}{A^2} + \sum\frac{K}{A^2}\right)\right\} \Big/ \sum\frac{L}{A} \tag{31}$$

where P_{gas} is the gas pressure at the last downstream node and A is the area of the gas-water interface. $\Sigma K/A^2$ and $\Sigma L/A$ are the integrated losses and inertial length for the flow path between the gas-water interface and the pool. The pool area is assumed to be infinitely large ($A_{pool} = \infty$), so that the velocity in the pool is negligible, and the term $1/A^2_{pool}$ is zero. Gravitation is also neglected. The values A, $\Sigma K/A^2$ and $\Sigma L/A$ are users' inputs as a function of the volume of water in the line as measured from the discharge (pool) end.

$\partial w/\partial t$ is integrated once to get the flowrate, w, and a second time to get the displacement, z.

2.2.2 Thrust Calculation

As mentioned previously, the air system description only approximates the actual geometry. The resulting forces computed by equation (18) will only be approximate if the degree of approximation of the actual geometry is significant. For some cases, including the segment with the GE x-quencher, the degree of approximation will be appreciable. The downthrust on the discharge device due to water clearing is, however, one of the more limiting loads. To compute this specific load, provisions are made in the model that are not affected by gas-system approximation. In these cases, the water thrust on the discharge device can be computed from a formula obtained by manipulating the conservation of momentum equation for the water:

$$g_c F = (z_w - z_o) \frac{\partial w}{\partial t} - w^2/(\rho_w A_c) \tag{32}$$

where z_w is the axial length of the water column and z_o is the distance from the discharge to the point where the flow has turned 90° such that the contribution to axial force is no longer significant (Figure 2-4).

Finally, if there is no turn (such as a straight pipe) z_o is zero and the thrust has an additional term

$$g_c F_j = w^2/\rho_w A_d \tag{33}$$

where A_d is the exit area. The total thrust is then $F + F_j$.

It should be noted that if there are turns in the pipe upstream of the ramshead or quencher, the water thrust calculation from equation (21) will not be correct when the gas-water interface is upstream of the turn. However, the peak force does not occur until the interface is turning the corner in the discharge device. After the interface has moved downstream past this upstream elbow, the calculations are valid.

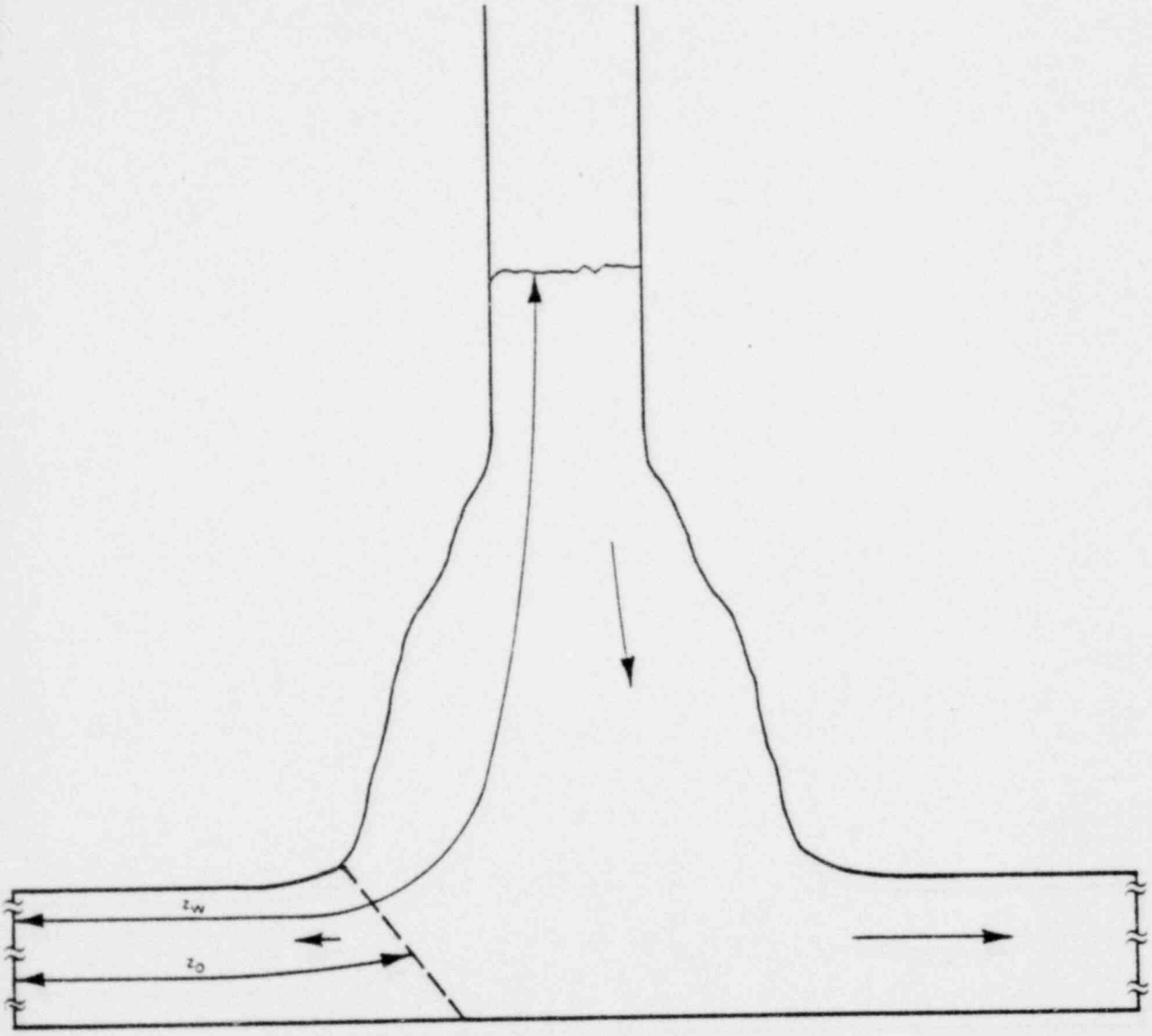

Figure 2-4. Discharge Device

3. VERIFICATION

In addition to the usual checks for reasonable and consistent results, the new analytical model was verified by:

A. Comparison with a previous model

B. Comparison with Quad Cities plant data

C. Comparison with Monticello plant data (ramshead)

D. Mass balances.

3.1 COMPARISON WITH A PREVIOUS MODEL

If the new model were used for a constant area pipe (including the water leg) with uniform friction and no condensation, the results would be expected to be similar to the older model that had these limitations.[4] The only significant difference is the expanding nodal grid of the newer model. In the older model only the original air leg was nodalized and new nodes were not added as the water moved out. Figure 3-1 shows a comparison of the line pressure at a point corresponding to the air-water interface. Until the water starts to move, the two modes are identical. After that, the older model gives slightly higher values as expected. Other results show similar good agreement. The older model predicts a maximum pipe pressure (which occurs next to the S/RV) that is 10 psia or 2% higher than the new model. Maximum segment forces on the first-wave pass are identical.

Comparison with the old model provides confidence that no errors were introduced into the basic structure during the modification process. The old model was verified by hand calculations, which indicated that within the assumptions made, the mass and energy balances and water flow calculations were correct.

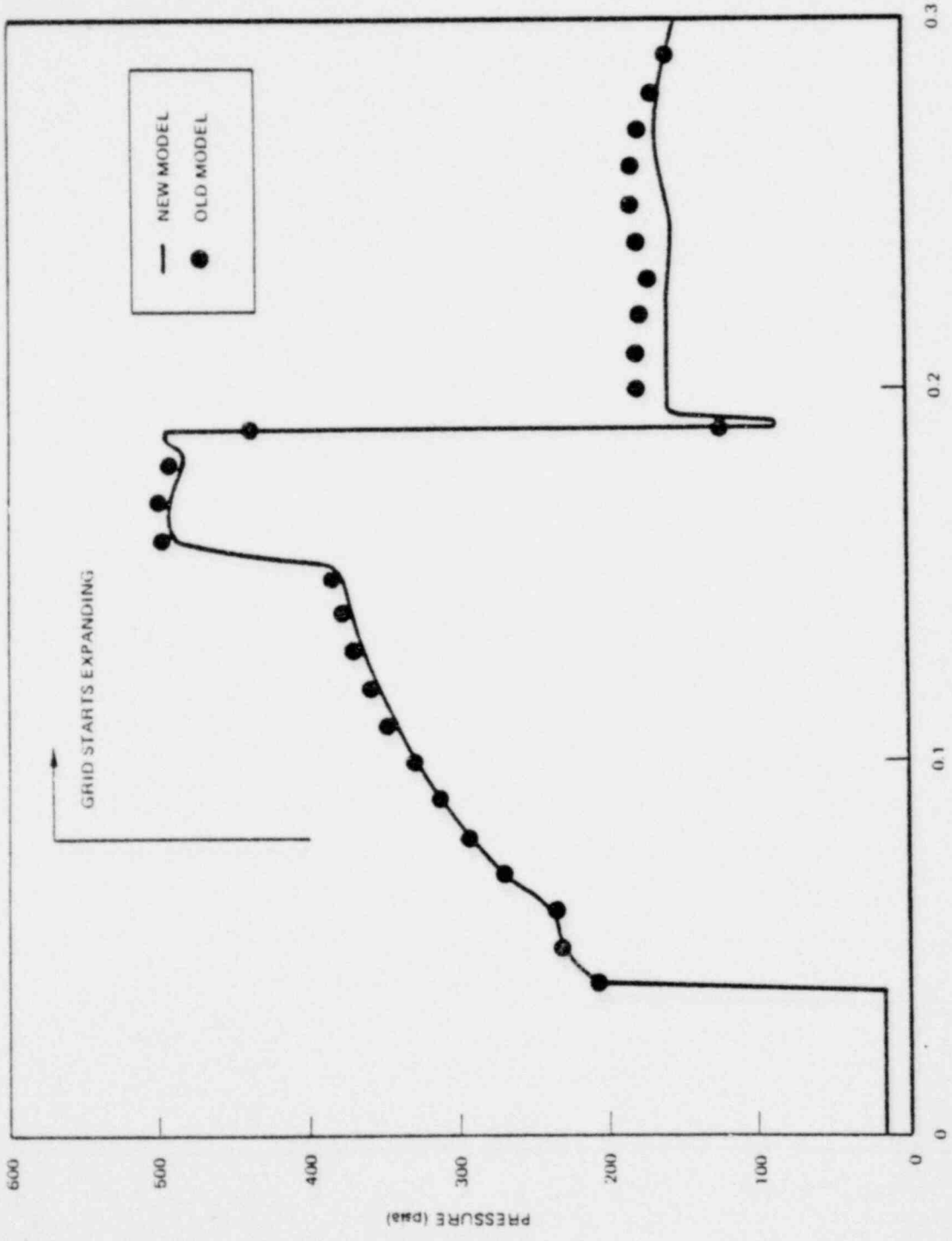

Figure 3-1. Comparison with Old Model

.2 COMPARISON WITH QUAD CITIES TEST DATA

he pipe pressure was measured in the Quad Cities 2 power plant at a point ust above the initial air-water interface.(5) Table 3-1 shows key parameters or this test. Figure 3-2 shows comparisons with the test data using arametric variation of inside wall condensation. Without any condensation, he peak pressure is overpredicted by 35%. With condensation and an inside urface condensation heat transfer coefficient of 10,000 Btu/hr-ft^2/°F, the eak and the curve before the peak are well predicted. After the peak, the eviation is larger. This is caused in part by the assumed boundary condi- ion that the exit flow goes sonic when the water clears. In fact, the air ubble in the pool probably offers some backpressure to the S/RVDL air as he bubble grows. The final steady-state prediction is good.

eat transfer coefficients in the 10,000 to 20,000 range are considered easonable during the S/RV charging transient. The pipe inside surface is nitially dry and condensation will resemble dropwise condensation. As steam s condensed, the water film will remain thi since it is swept down the pipe y the high velocity steam flow. The small change in pressure when the heat ransfer coefficient is doubled from 10,000 to 20,000 indicates that the rimary resistance to heat transfer is wall conduction resistance.

.3 COMPARISON WITH MONTICELLO TEST DATA

easurements during a June 1976 S/RV test at the Monticello plant include ipe pressures and stresses in portions of the piping and support structure. hese measurements provide the basis for model-data comparison for pipe pres- ure, wave forces, and thrust due to water clearing.

he important model parameters from the Monticello test are shown in Table 3-2. igure 3-3 presents a comparison of predicted pressure histories with test ata at two pressure taps for an initially cold S/RV line. P1 is located ne foot downstream from the S/RV and P3 is halfway down the line. A con- ensation heat transfer coefficient of 10,000 Btu/hr-ft^2-°F was used, which s the value found optimum to predict the Qua. Cities 2 test data. At tap P1,

Table 3-1

PARAMETERS FOR QUAD CITIES 2 PREDICTION

Air Length*	74 ft
Initial Water Volume*	7 ft^3
Pipe Diameter*	8 inches
Initial Pipe Temp	150°F
Initial Air Density	0.07 lbm/ft^3
Initial Air Pressure	14.7 psig
Steamline Pressure*	980 psig
Steamline Density*	2.19 lbm/ft^3
Valve Opening Time (Simple Ramp)	0.02 seconds
Valve Flow Rate*	152.7 lbm/sec
Friction Factor	0.029

DISCHARGE HYDRAULIC CHARACTERISTICS

Volume Water Filled ft^3	Interface Flow Area ft^3	$\sum \frac{K}{A^2}\left[\frac{1}{ft^4}\right]$	$\sum \frac{L}{A}\left[\frac{1}{ft}\right]$
0.	0.634	2.48	1.0
0.97	0.634	2.57	3.41
1.97	0.3174	4.55	5.51
9.905	0.3174	10.41	84.27

*Based on actual measurements or known test conditions. Other inputs are estimated.

Figure 3-2. Comparison of Model with Quad Cities 2 Test Data (Company Proprietary)

Table 3-2

PARAMETERS FOR MONTICELLO PREDICTION (Company Proprietary)

Figure 3-3. Model-Data Pressure Comparison Monticello Ramshead Test (TSN1, Run 14) (Company Proprietary)

the model predicts the steady state well and is about 15-20% high at the peak. In the early portion, however, the model overpredicts the data at P1. The pressure tap is located only one foot downstream of and is probably in the wake region the S/RV as the flow expands from the S/RV throat area to the pipe area. If the tap is in the wake region, it will not accurately measure free stream static pressure. As the backpressure is increased, the wake region becomes shorter and the tap is in the attached flow region and gives a noisy but more accurate reading. This interpretation is supported by the behavior at tap P3, which does not show such a significant discrepancy at the start of the transient.

Predictions of the pressure at P1 were also made for a hot pipe test. The pipe wall had been heated by a previous S/RV discharge; the pipe was not uniformly hot, however, since reflood after the S/RV closure cooled the lower half of the pipe. These results are shown in Figure 3-4. Two different water leg lengths - 2 feet and 10 feet of overshoot - are predicted. The actual water position could not be accurately determined but was estimated to be between ' and 10 feet above the pool surface, with 2 ft being the best estimate. The prediction is about 25% higher than the data - worse agreement than for the cold pipe. The cause of this discrepancy is unknown.

(Company Proprietary)

test. A model prediction for the stress in the S/RV branch from the steam line using wave forces from the present model and a structured computer pro-

(Company Proprietary)

value and considered good agreement (Figure 3-5).

Water clearing thrust on the ramshead was measured in the same test, indicating

(Company Proprietary)

comparison of predicted to measured stresses at one location is shown in Figure 3-6; peak force was determined by averaging this stress and the measured stress at two other locations. The discrepancy could be caused by the gas-water interface in the pipe being unstable (Taylor Instability) and the water not clearing as a simple slug as modeled.

Figure 3-4. S/RV Pipe Pressure Comparison (Hot Pipe, Elevated Water Level Condition) (Company Proprietary)

Figure 3-5. Comparison Between Measured and Calculated Stress Time History at SG 39A (Company Proprietary)

Figure 3-6. Moment-Time History at SG 41 Monticello Test
(Company Proprietary)

3.4 MASS BALANCES

As with any finite difference procedure, the method of characteristics contains numerical errors resulting from numerical approximations of the governing equations. In the model, it is easy to check overall mass conservation of the gases in the line just before water clearing. The total mass should be the initial air mass plus the mass of steam that has flowed into the pipe,

$$\text{Expected Mass} = m_{air} + \int_0^t \dot{m}_{steam}\, dt \tag{34}$$

The code computes, for this purpose, a volume average density, ρ_{ave}. The computed mass is

$$\text{Computed Mass} = \rho_{ave}\, \text{Vol}, \tag{35}$$

where Vol is the gas volume at the instant before water clearing. After water clearing, mass has flowed out of the pipe and the calculation becomes more complicated. The % mass unbalance is defined as

$$\text{Unbalance} = \frac{\text{Expected Mass} - \text{Computed Mass}}{\text{Expected Mass}} \tag{36}$$

For the model, mass unbalances were found to be less than 6% (computed mass is less than expected mass), and it is expected that pressure and force results are uncertain because of numerical errors to about the same degree. This is considered satisfactory for this method.

The mass unbalances were found to be primarily sensitive to valve opening time (Figure 3-7). The number of nodes has little effect in the 100-150 range normally used. The cause of the opening time sensitivity apeears to be the numerical approximation of shock waves. This unbalance is proportional to the shock strength, which, in turn, depends upon the valve opening time.

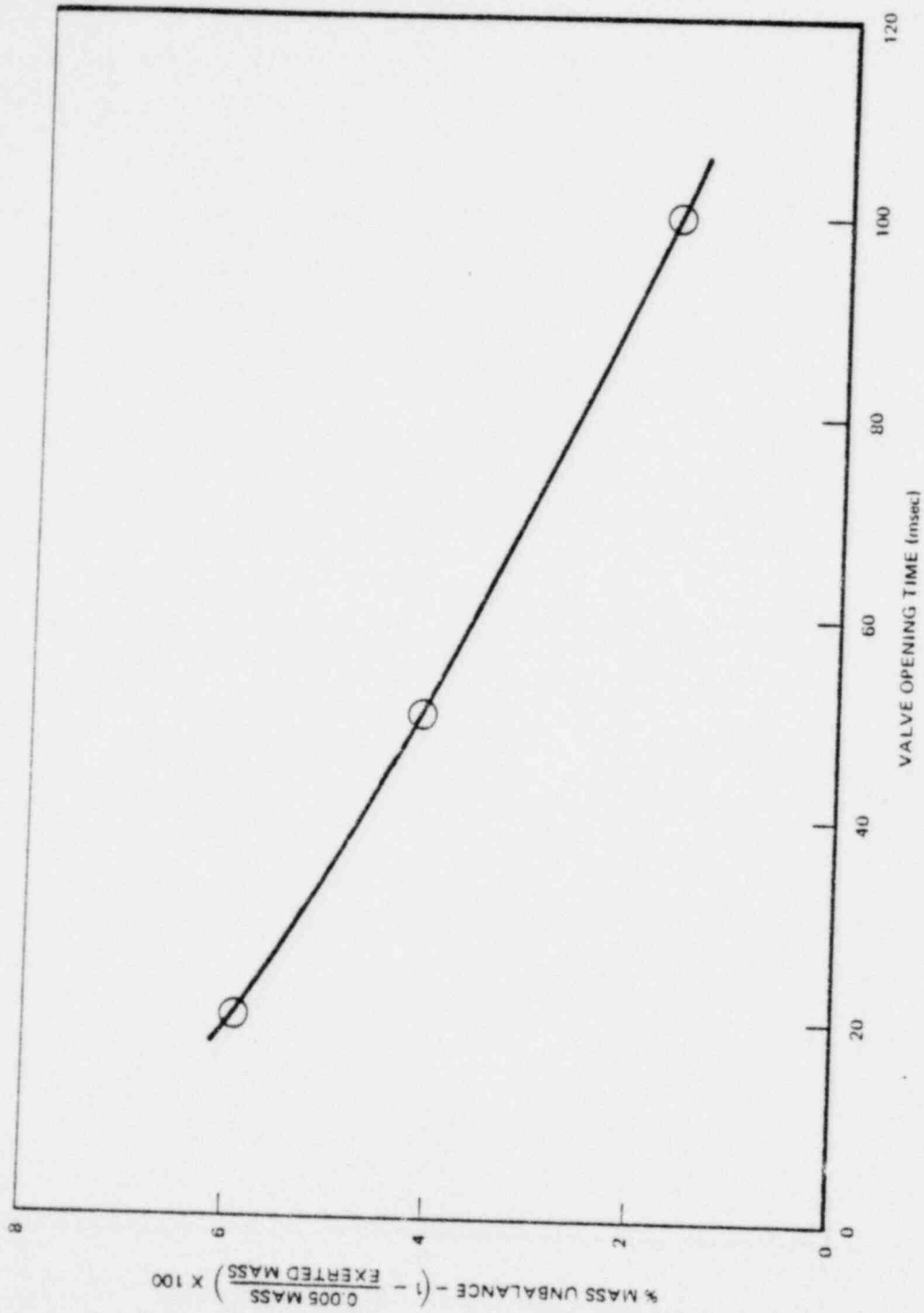

Figure 3-7. Mass Unbalance as a Function of Valve Opening Time

4. REFERENCES

1. S.A. Sandoz, *Amplitude Response of Fluidic Transmission Lines*, PhD Thesis, Stanford University, Department of Mechanical Engineering, 1973.

2. F. Kreith, *Principles of Heat Transfer*, International Textbook, 1958.

3. F.J. Moody, *Fluid Reaction and Impingement Loads*, Specialty Conference on Structural Design of Nuclear Power Plants, American Society of Civil Engineers, New York, December 17-18, 1973.

4. P. Valandani, *Safety Relief Valve Discharge Analytical Models*, NEDE-20942-P, May 1975.

5. J.L. McCready, et al., *Steam Vent Clearing Phenomena and Structural Responses of the BWR Torus (Mark I Containment)*, NEDO-10859, April, 1973.

6. A.H. Shapiro, *Compressible Fluid Flow*, Ronald Press, 1953.

7. E.A. Buzek, et al., *Final Report-In-Plant Safety/Relief Valve Discharge Load Test - Monticello Plant*, NEDC-21581-P, August 1977.

APPENDIX A
NOMENCLATURE

	Pipe cross-sectional area
	Sound speed
F_1, F_2, F_3	Functions in method of characteristics
	Force constant
c	Specific enthalpy
	Total specific enthalpy
o	Wall heat transfer coefficient
wall	Internal energy
	Ratio of specific heats, c_p/c_v
	Mass flowrate
h'' c	Condensation mass flux
M	Mach number
m	Mass of fluid
P	Pressure
P_w	Pipe wetted perimeter
$\dot{Q}''$	Heat flux
$\dot{Q}''_c$	Heat flux into pipe wall due to condensation
r	Radius
r_1	Pipe radius
R	Gas constant
s	Specific entropy
t	Time
Δt	Time step
T	Temperature, °F or °R, as used
u	Velocity of gas
V	Velocity
V_s	Absolute shock velocity
V_{sr}	Relative shock velocity
w	Water flowrate
z	Axial distance along pipe

z_w	Length of water column
z_o	Length of water after 90° turn
z_{ls}	Length of water column in last segment
α'	Thermal diffusivity
α, β, γ	Functions in method of characteristics
$\lambda_1, \lambda_2, \lambda_3$	Transformation factors used in method of characteristics derivation
ρ	Density
τ_w	Wall shear stress
$\Sigma \frac{K}{A^2}$	Cumulative loss coefficient
$\Sigma \frac{L}{A}$	Cumulative inertial length

Subscripts

E	Entrance condition
sat	At saturation
wall	At wall
y	Downstream of shock (high P)
x	Upstream of shock (low P)
seg	Segment
J	Jet
i	Gas node

APPENDIX B
BASIC GAS DYNAMIC EQUATIONS

Consider the control volume shown in Figure B-1.

Conservation of Mass

$$\text{Outflow} - \text{inflow} + \text{increase of storage} = 0$$

$$\left(\rho + \frac{\partial \rho}{\partial z}\,dz\right)\left(u + \frac{\partial u}{\partial z}\,dz\right)\left(A + \frac{dA}{dz}\,dz\right) + \dot{m}''_c P_w\,dz - \rho u A + \frac{d}{dt}(\rho A\,dz) = 0 \qquad (1)$$

Expanding, dropping terms involving dz^2 or dz^3 and dividing by Adz gives:

$$\rho\frac{\partial u}{\partial z} + u\frac{\partial \rho}{\partial z} + \frac{\partial \rho}{\partial t} + \rho\frac{u}{A}\frac{dA}{dz} + \dot{m}''_c\frac{P_w}{A} = 0 \qquad (2)$$

Conservation of Momentum

$$\text{Outflow} - \text{inflow} + \text{increase storage} = \Sigma F_x$$

$$\left(\rho + \frac{\partial \rho}{\partial z}\,dz\right)\left(u + \frac{\partial u}{\partial z}\,dz\right)^2\left(A + \frac{dA}{dz}\,dz\right) + \dot{m}''_c u P_w\,dz - \rho u^2 A + \frac{\partial}{\partial t}(\rho A u\,dz) =$$

$$g_c\left\{-\tau_w P_w\,dz + PA - \left(P + \frac{\partial P}{\partial z}\,dz\right)\left(A + \frac{dA}{dz}\,dz\right) + P\frac{dA}{dz}\,dz\right\} \qquad (3)$$

Expanding, dropping terms involving dz^2, dz^3, or dz^4 and noting that several terms combine due to conservation of mass one gets:

$$\rho u\frac{\partial u}{\partial z} + \rho\frac{\partial u}{\partial t} + g_c\frac{\partial P}{\partial z} + g_c\tau_w\frac{P_w}{A} = 0 \qquad (4)$$

Conservation of Energy

Outflow - inflow + increase storage = 0

$$\left(\rho + \frac{\partial \rho}{\partial z} dz\right)\left(u + \frac{\partial u}{\partial z} dz\right)\left(A + \frac{dA}{dz} dz\right)\left(h_o + \frac{\partial h_o}{\partial z} dz\right) + m''_c h_o P_w dz$$

$$+ \dot{Q}'' P_w dz - \rho u A h_o + \frac{d}{\partial t}\left(PA\, dz\, i_o\right) = 0 \qquad (5)$$

Expanding and dropping terms in dz^2, dz^3, and dz^4, noting that the internal energy

$$i_o = h_o - P/\rho \qquad (6)$$

and incorporating conservation of mass gives

$$\rho \frac{\partial h_o}{\partial t} + \rho u \frac{\partial h_o}{\partial z} - \frac{\partial P}{\partial t} + \dot{Q}'' \frac{P_w}{a} = 0 \qquad (7)$$

here h_o is the total enthalpy, static plus kinetic energy.

The conservation of mass, momentum, and energy equations resulted in three equations in four unknowns, ρ, P, u and h. The properties of pure substances are used to close the problem.

Noting that

$$h_o = h + \frac{u^2}{2g_c} \qquad (8)$$

Equations (4), (7), and (8) combine to give

$$\frac{\partial h}{\partial z} + u\frac{\partial h}{\partial z} - \frac{1}{\rho}\left(\frac{\partial P}{\partial t} + u\frac{\partial P}{\partial t}\right) = u\frac{{}_{t}P_{w}}{\partial A} - \frac{Q''P_{w}}{\partial A} \qquad (9)$$

h can be eliminated as follows

For a simple compressible substance

$$h = h(P,\rho) \qquad (10)$$

$$s = s(P,\rho) \qquad (11)$$

Differentiating

$$dh = \left(\frac{\partial h}{\partial P}\right)_{\rho} dP + \left(\frac{\partial h}{\partial \rho}\right)_{P} d\rho \qquad (12)$$

$$ds = \left(\frac{\partial s}{\partial P}\right)_{\rho} dP + \left(\frac{\partial s}{\partial \rho}\right)_{P} d\rho \qquad (13)$$

also

$$\left(\frac{\partial h}{\partial t}\right)_{z} = \left(\frac{\partial h}{\partial P}\right)_{\rho}\left(\frac{\partial P}{\partial t}\right)_{z} + \left(\frac{\partial h}{\partial \rho}\right)_{P}\left(\frac{\partial \rho}{\partial t}\right)_{z} \qquad (14)$$

$$\left(\frac{\partial h}{\partial z}\right)_{t} = \left(\frac{\partial h}{\partial P}\right)_{\rho}\left(\frac{\partial P}{\partial z}\right)_{t} + \left(\frac{\partial h}{\partial \rho}\right)_{P}\left(\frac{\partial \rho}{\partial z}\right)_{t} \qquad (15)$$

The Gibbs equation may be written as

$$T\,ds = dh - \frac{1}{\rho}\,dP \qquad (16)$$

Equations (16), (13), and (12) may be combined to give

$$\left(\frac{\partial h}{\partial \rho}\right)_P = T\left(\frac{\partial s}{\partial \rho}\right)_P \tag{17}$$

$$\left(\frac{\partial h}{\partial P}\right)_\rho - \frac{1}{\rho} = T\left(\frac{\partial s}{\partial P}\right)_\rho \tag{18}$$

Also, for a constant entropy process (ds = 0) equations (13) shows,

$$\frac{dP}{d\rho} = \left(\frac{\partial P}{\partial \rho}\right)_s = \left(\frac{\partial s}{\partial \rho}\right)_P \Big/ \left(\frac{\partial s}{\partial P}\right)_\rho \tag{19}$$

and

$$\left(\frac{\partial P}{\partial \rho}\right)_s = C^2/g_c \quad \text{(See Reference 6, Shapiro)} \tag{20}$$

Combining Equations (20), (19), (18), (17), (15), (14), and (9) gives

$$\frac{\partial P}{\partial t} + u\frac{\partial P}{\partial z} - \frac{C^2}{g_c}\left(\frac{\partial \rho}{\partial t} + u\frac{\partial \rho}{\partial z}\right)$$

$$= (u\tau_w P_w/\rho A - \dot{Q}'' P_w/\rho A)\Big/\left(\left(\frac{\partial h}{\partial p}\right)_\rho - \frac{1}{\rho}\right) \tag{21}$$

Rewriting the conservation equations,

$$\frac{\partial \rho}{\partial t} + u\frac{\partial \rho}{\partial z} + \rho\frac{\partial u}{\partial z} = \Gamma_1(z,t) \tag{22}$$

$$\frac{\partial u}{\partial t} + u \frac{\partial u}{\partial z} + \frac{g_c}{\rho} \frac{\partial P}{\partial z} = F_2(z,t) \tag{23}$$

$$\frac{\partial P}{\partial t} + u \frac{\partial P}{\partial z} + \left(\frac{-C^2}{g_c}\right)\left(\frac{\partial \rho}{\partial t} + u \frac{\partial \rho}{\partial z}\right) = F_3(z,t) \tag{24}$$

ere:

$$F_1(z,t) = - \frac{\rho u}{A} \frac{dA}{dz} - \dot{m}''_c \frac{P_w}{A} \tag{25}$$

$$F_2(z,t) = - g_c \left(\frac{\tau_w}{\rho} \frac{P_w}{A}\right) \tag{26}$$

$$F_3(z,t) = \frac{u\tau_w P_w - \dot{Q}''(z,t) P_w}{\rho A\left(\left(\frac{\partial h}{\partial p}\right)_\rho - \frac{1}{\rho}\right)} \tag{27}$$

ultiply equations (22), (23), and (24) by the undetermined constants
λ_1, λ_2, λ_3, and add together:

$$\lambda_3 \frac{\partial P}{\partial t} + \left(\lambda_1 + \lambda_3 \left(\frac{-C^2}{g_c}\right)\right)\frac{\partial \rho}{\partial t} \quad \lambda_2 \frac{\partial u}{\partial t} + \left(\lambda_2 \frac{g_c}{\rho} + \lambda_3 u\right) \frac{\partial P}{\partial z}$$

$$+ \left(\lambda_1 u - \lambda_3 u \frac{C^2}{g_c}\right) \frac{\partial P}{\partial z} + (\lambda_1 \rho + \lambda_2 u) \frac{\partial u}{\partial z} = \lambda_1 F_1 + \lambda_2 F_2 + \lambda_3 F_3 \tag{29}$$

egarding:

$$\begin{aligned} P &= P(z,t) \\ u &= u(z,t) \\ \rho &= \rho(z,t) \end{aligned} \tag{30}$$

It can be written

$$\frac{\partial P}{\partial z} = \frac{dP}{dz} - \frac{\partial P}{\partial t}\frac{dt}{dz}$$

$$\frac{\partial u}{\partial z} = \frac{du}{dz} - \frac{\partial u}{\partial t}\frac{dt}{dz} \qquad (31)$$

$$\frac{\partial \rho}{\partial z} = \frac{d\rho}{dz} - \frac{\partial \rho}{\partial t}\frac{dt}{dz}$$

and eliminate $\frac{\partial P}{\partial z}$, $\frac{\partial u}{\partial z}$, $\frac{\partial \rho}{\partial t}$ from (29). Then, (29) becomes

$$\left[\lambda_3 - \left(\lambda_2\frac{g_c}{\rho} + \lambda_3 u\right)\frac{dt}{dz}\right]\frac{\partial P}{\partial t} + \left[\lambda_1 - \lambda_3\frac{C^2}{g_c} - u\left(\lambda_1 - \lambda_3\frac{C^2}{g_c}\right)\frac{dt}{dz}\right]\frac{d\rho}{\partial t}$$

$$+\left[\lambda_2 - \left(\lambda_1\rho + \lambda_2 u\right)\frac{dt}{z}\right]\frac{\partial u}{\partial t} + \left(\lambda_2\frac{g_c}{\rho} + \lambda_3 u\right)\frac{dP}{dz} + u\left(\lambda_1 - \lambda_3\frac{C^2}{g_c}\right)\frac{d\rho}{dz} \qquad (32)$$

$$+ (\lambda_1\rho + \lambda_2 u)\frac{du}{dz} = \lambda_1 F_1 + \lambda_2 F_2 + \lambda_3 F_3$$

The partial derivatives will vanish from (32) if λ_1, λ_2 and λ_3 are chosen properly so that the coefficients of $\frac{\partial P}{\partial t}$, $\frac{\partial \rho}{\partial t}$ and $\frac{\partial u}{\partial t}$ are zero. Formally,

$$\frac{-g_c}{\rho}\frac{dt}{dz}\lambda_2 + \left(1 - u\frac{dt}{dz}\right)\lambda_3 = 0 \qquad (33)$$

$$\left(1 - u\frac{dt}{dz}\right)\lambda_1 \frac{-C^2}{g_c}\left(1 - u\frac{dt}{dz}\right)\lambda_3 = 0 \qquad (34)$$

$$-\rho \frac{dt}{dz} \lambda_1 + \left(1 - u \frac{dt}{dz}\right) \lambda_2 = 0 \tag{35}$$

he system (33), (34), (35) has a solution only if the coefficient determinant s zero, or,

$$\left(1 - u \frac{dt}{dz}\right) \left[\left(-C^2 + u^2\right) \left(\frac{dt}{dz}\right)^2 - 2u \frac{dt}{dz} + 1\right] = 0 \tag{36}$$

ermissible solutions for $\frac{dt}{dz}$ give the characteristics lines

$$\frac{dt}{dz} = \frac{1}{u} \tag{37}$$

$$\frac{dt}{dz} = \frac{u + \sqrt{g_c \frac{C^2}{g_c}}}{u^2 + g_c \left(\frac{-C^2}{g_c}\right)} = \frac{1}{u - C} \tag{38}$$

$$\frac{dt}{dz} = \frac{u - \sqrt{g_c \frac{C^2}{g_c}}}{u^2 + g_c \frac{C^2}{g_c}} = \frac{1}{u + C} \tag{39}$$

f (37), (38), and (39) are substituted into (33), (34), and (35), it is ound that

$$\frac{\lambda_2}{\lambda_3} = 0 \; ; \; \frac{\lambda_1}{\lambda_3} = 0 \; ; \qquad \text{for } \frac{dt}{dz} = \frac{1}{u} \tag{40}$$

$$\frac{\lambda_2}{\lambda_3} = -\frac{gC}{g_c} \; ; \; \frac{\lambda_1}{\lambda_3} = \frac{C^2}{g_c} \; , \qquad \text{for } \frac{dt}{dz} = \frac{1}{u - C} \tag{41}$$

$$\frac{\lambda 2}{\lambda 3} = \frac{\rho C}{g_c} \quad ; \quad \frac{\lambda 1}{\lambda 3} = \frac{C^2}{g_c} \quad ; \qquad \text{for} \quad \frac{dt}{dz} = \frac{1}{u + C} \tag{42}$$

Finally, if (40), (41), and (42) are substituted into (32), recalling that the partial derivative coefficients are zero, ordinary differential equations are obtained for

$$dP + \frac{\rho C}{g_c}\, du = \alpha dt \qquad \text{on} \quad \frac{dt}{dz} = \frac{1}{u + c} \tag{43}$$

$$dP - \frac{\rho C}{g_c}\, du = \beta dt \qquad \text{on} \quad \frac{dt}{dz} = \frac{1}{u - c} \tag{44}$$

$$d\rho - \frac{g_c}{C^2}\, dP = \gamma dt \qquad \text{on} \quad \frac{dt}{dz} = \frac{1}{u} \tag{45}$$

where

$$\alpha = \frac{C^2}{g_c} F_1 + \frac{\rho C}{g_c} F_2 + F_3 \tag{46}$$

$$\beta = \frac{C^2}{g_c} F_1 - \frac{\rho c}{g_c} F_2 + F_3 \tag{47}$$

$$\gamma = \frac{-g_c}{C^2} F_3 \tag{48}$$

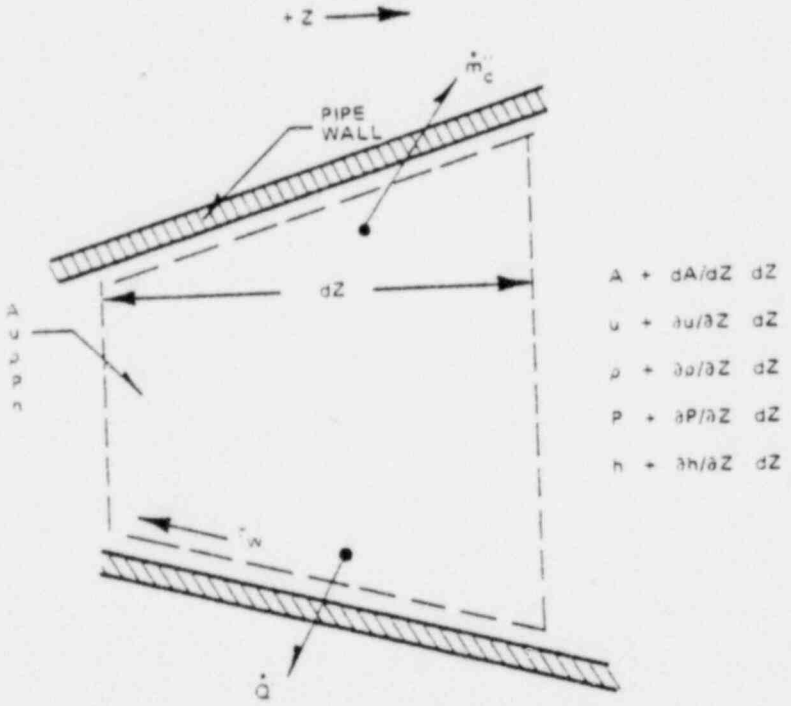

Figure B-1. Gas System Differential Control Volume

APPENDIX C

MASS BALANCE ACROSS NORMAL SHOCK

Figure A-1 shows a control volume of the region between nodes n and n+1. It is assumed that the flow is quasi-steady upstream and downstream of the shock. Then conservation of mass gives

$$\dot{m}_2 - \dot{m}_1 + \frac{d}{dt}\left(XA_n\rho_n + (\Delta z - z)\ \rho_{n+1}A_n\right) = 0$$

$$\dot{m}_2 - \dot{m}_1 + A\rho_n\frac{dx}{dt} - \frac{dx}{dt}\ \rho_{n+1}A = 0$$

or since

$$\frac{dx}{dt} = -V_s$$

and

$$\dot{m} = \rho VA$$

$$\rho_{n+1}u_{n+1}A_{n+1} = \rho_n u_n A_n - V_s A_n\ (\rho_{n+1} - \rho_n)$$

$$u_{n+1} = \rho_n u_n A_n - V_s A_n(\rho_{n+1} - \rho_n) \Big/ \rho_{n+1}u_{n+1}$$

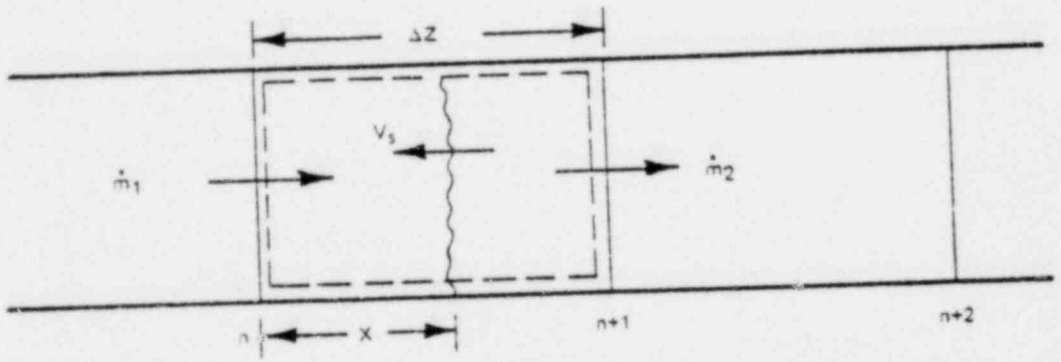

Figure C-1. Moving Shock Control Volume